

# A Practical Approach to Indoor Path Loss Modeling Based on Deep Learning

Shengjie Ma, Hong Cheng, and Hyukjoon Lee\*

Department of Computer Engineering, Kwangwoon University, Seoul, Korea  
mashengjie@kw.ac.kr, chenghong@kw.ac.kr, hlee@kw.ac.kr

## Abstract

Deep learning has become one of the most powerful prediction approaches, and it can be used to solve classification and regression problems. We present a novel deep learning-based indoor Wi-Fi path loss modeling approach. Specifically, we propose a local area multi-line scanning algorithm that generates input images based on measurement locations and a floor plan. As the input images contain information regarding the propagation environment between the fixed access points (APs) and measurement locations, a convolutional neural network (CNN) model can be trained to learn the features of the indoor environment and approximate the underlying functions of the Wi-Fi signal propagation. The proposed deep learning-based indoor path loss model can achieve superior performance over 3D ray-tracing methods. The average root mean square error (RMSE) between the predicted and measured received signal strength values in the two scenarios is 4.63 dB.

**Category:** Artificial Intelligence

**Keywords:** Deep learning; Indoor path loss modeling; Convolutional neural networks

## I. INTRODUCTION

As indoor wireless communication using Wi-Fi has become a necessity in day-to-day life, the provision of Wi-Fi access in public and private buildings is becoming increasingly important. Access points (APs) must be carefully positioned to provide reliable wireless connectivity to users. Path loss prediction plays a crucial role in determining the optimal placement of APs. While a number of relevant studies have been conducted in this area, the majority of the path loss prediction models have failed to reach the accuracy level needed for practical use. This is mainly due to the diversity of the usage scenarios and environmental characteristics [1-3]. The complexity and unpredictability of path loss prediction in indoor

environments are caused by various factors, including line of sight (LoS) and non-LoS (NLoS) propagation, human movement, furniture placement, and the construction materials used. Consequently, the received signal strength (RSS) of the AP varies with time and location.

Researchers have developed traditional indoor path loss prediction models using deterministic and/or empirical methods. Deterministic models such as ray-tracing methods employ physical laws to estimate the power loss of radio signals [1]. However, they require an excessive amount of computational time, and detailed information regarding the radio environment is typically unavailable. Empirical models including the closed-in model and alpha-beta-gamma model are based on regression with field measurement data, in which the TR-separation (the distance

---

**Open Access** <http://dx.doi.org/10.5626/JCSE.2021.15.2.84>

<http://jcse.kiise.org>

This is an Open Access article distributed under the terms of the Creative Commons Attribution Non-Commercial License (<http://creativecommons.org/licenses/by-nc/4.0/>) which permits unrestricted non-commercial use, distribution, and reproduction in any medium, provided the original work is properly cited.

Received 30 April 2021; Accepted 31 May 2021

\*Corresponding Author

between the transmitter and the receiver) and frequency are generally considered [4]. Although empirical models usually yield less accurate prediction results than the deterministic models, the simplicity of the empirical methods has made them popular, and they require fewer computational resources.

Neural networks have demonstrated good performance on path loss predictions in indoor environments [3]. Neural network-based methods do not require the precise environmental information required by deterministic methods, such as the electromagnetic (EM) characteristics of the building materials. However, there are some features that should be provided for the path loss prediction, such as information on the propagation environment, including distance, the frequency of the carrier wave, and terrain information [5]. Feature extraction algorithms, such as that described by Yang and Lee [6], should be designed carefully to obtain the appropriate features, which makes it difficult to achieve highly accurate path loss modeling based on neural networks.

Deep learning models such as convolutional neural networks (CNNs) can easily employ enormous amounts of available data and parallel computational power to achieve significantly improved performance in natural language processing, computer vision, and many other application domains [7]. CNN models can be trained to learn the features related to the propagation environment from the input data and underlying representations of the input data without the need for complex data pre-processing.

In this study, a deep learning-based path loss modeling method for 5.8 GHz Wi-Fi is proposed. This proposed system can predict the RSS more accurately than the 3D ray-tracing method. Based on the floor plan of a building where the field measurement data have been collected, a new kind of CNN input image that can represent the environment and radio propagation information is generated by the proposed local area multiple-line scanning (LAMS) algorithm. The LAMS algorithm can generate CNN input images containing information on the local area of a certain indoor environment in which the AP and the measurement points are located.

The rest of this paper is organized as follows. Section II presents a review of the related work on path loss modeling. A general introduction of CNN is provided in Section III-A. Next, the CNN-based path loss modeling system is illustrated in Section III-B. The measurement environment and data collection are then presented in Section III-C. The LAMS input image generation algorithm is proposed in Section III-D. The design of the proposed CNN-based path loss model is illustrated in Section III-E. In Section IV, the proposed deep learning-based path loss model is evaluated in two experimental test scenarios, where it is demonstrated to have high performance by which it outperforms 3D ray-tracing methods. Finally, Section V concludes this paper and presents future work.

## II. RELATED WORK

### A. Deterministic Models

The most common approach in deterministic indoor path loss prediction is ray-tracing methods. Ray-tracing is used to model the physical propagations of wireless signals by simulating the geometrical optics, including reflection, refraction, and others. There are two major types of ray-tracing methods: the brute force ray launching method and the image method [8]. The brute force method relies on a ray shooting in all directions from the transmitter, which requires numerous ray-object intersection tests and extensive data storage. Meanwhile, the image method associates virtual sources with every obstacle and calculates their effect on transmission based on wave propagation rules. Therefore, the image method is preferable due to its practical appeal and reduced computational complexity. One study used the image method to estimate the path loss based on the basic two-ray model for the indoor NLoS corridor scenario at 2.4 GHz frequency [8]. A generalized ray-tracing model that includes diffraction loss using both knife-edge diffraction and scattering loss has been proposed as an improvement over N rays [1].

However, due to the use of the knife-edge diffraction model, diffraction and scattering losses calculated from empirical models lead to bigger prediction deviations after a certain distance. In [9], a 3D ray-tracing method for path loss modeling at 15 GHz in indoor corridor scenarios is proposed which takes into account a direct path, specular reflection paths, and scattering paths. This 3D ray-tracing method also includes the antenna modeling components (the gain and polarization of the antenna), environment modeling components (the structure of the propagation environment, the permittivity and conductivity of all objects, and the location of Tx/Rx), and the 3D ray-based channel model components (type of path, i.e., direct path, reflection path, or scattering path, as well as path delay and 3D angular properties). In [10], a 3D ray-tracing approach is used to generate propagation models in the high-speed train tunnel and outdoor scenarios which consider the influences of the antenna and the other elements that affect the propagation including scattering, reflection, and diffraction. Two studies [11, 12] have reported on the developed 3D ray-optical tool, which can be used in the indoor scenario with modifications to the environment and the propagation parameters for a sub-6 GHz antenna.

For a given scenario, indoor deterministic path loss models based on the ray-tracing method typically make certain assumptions about the dominant elements affecting the wireless signal propagation, such as the maximum number of reflections of the transmission signal. To estimate the RSS, the empirical equation for the calculation of these factors may be used. The prediction accuracy of

deterministic models depends on whether there are enough site-specific parameters and whether the radio propagation environment information is available. However, such information is rarely available in practice, and the only thing that we can do is to apply the deterministic path loss model of a similar scenario. Another major drawback of deterministic models is that they require a tremendous amount of computational resources as well as time.

## B. Empirical Models

Empirical models are constructed from the field measurements taken in specific representative environments. In [2], the authors propose an indoor path loss model called the Tata Indoor Path Loss Model (T-IPLM) used for regular Wi-Fi operations within the 2.4–2.5 GHz band in India; this model considers the power loss coefficient due to distance, the LoS loss factor of walls (glass or wooden or temporary partitions) between the transmitter and the receiver. The total loss due only to walls and the floor attenuation factor are two parts in the T-IPLM. The floor attenuation factor is considered as a separate consideration in [2]. Although the simulation result shows that T-IPLM performs better than the popular empirical path loss models used in practice, such as ITU-R and the log-distance model, it must be given the loss factor of the building structure and the floor attenuation factor, which are difficult to calculate and estimate.

In [13], another indoor empirical path loss model is presented for the scenarios of a closed corridor, an open corridor, a classroom, and a computer lab. The log-distance path loss model together with log-normal shadowing, and the two-ray model are used to determine path loss equations for different scenarios. In [14], a d1-and-d2 path loss model is proposed where d1 and d2 are LoS and NLoS distances, respectively. This model can predict path loss when a mobile receiver is moving around the corners of a building in an indoor scenario with a carrier frequency of 5.25 GHz. In [15], a path loss model for wireless indoor office environments at the 5.8 GHz band is proposed. The path loss is modelled by characterizing the distance with a Gaussian random variable  $X$  due to the shadow fading by linear regression in addition to the log-distance path loss model. The path loss exponent  $n$  is fitted by the frequency using the power function and modelled as a frequency-dependent Gaussian variable as the standard deviation  $\sigma$  of  $X$ . El-Keyi et al. [16] present an indoor probabilistic path loss model for smart homes, which takes into account excess path loss caused by indoor propagation effects such as wall penetration, reflection, scattering, and diffraction effects, and a loss component is probabilistically added to the log-distance path loss model. This model does not require building topology and material knowledge, and the probability of the additional loss component depends only on the TR-separations, which is the distance between the transmitter and receivers.

Empirical models typically use the dominant factors that can affect radio propagation as features to model the path loss in a given scenario. To achieve higher accuracy, more features can be considered, such as the antenna height, the furniture distribution, and the building materials. These factors can also be added in the format of probability. The critical parameters, such as the path loss component and the standard deviation of Gaussian shadow fading, could be found by curve fitting with the measurement data. Compared to the deterministic models, the empirical models are derived from the RSS measurements, where the grid measurement of RSS in the indoor scenario must be performed. The empirical models have demonstrated satisfactory computational efficiency, and they are easy to apply to similar types of scenarios without complex modifications. However, since they are not built to be specific enough to each path loss modeling scenario, the prediction performance of the empirical methods is usually not better than that of the deterministic path loss modeling methods.

## C. ANN Models

Artificial neural networks, also known as ANNs or NNs, are computational models inspired by the structures and functions of biological neurons of intelligent organisms, and they have the ability to acquire knowledge through experience [6, 7, 17, 18]. Given inputs that contain enough appropriate information about the radio propagation environment, ANNs can learn the underlying function of a path loss using the measurement data as the training data set and then make predictions for arbitrary locations due to their so-called *generalization* capabilities.

In [19, 20], multilayer perceptron (MLP) networks and radial basis functions (RBF) networks are used to make predictions of RSSs in complex indoor environments. RBF networks and MLP networks are both nonlinear multilayer neural networks. An RBF network only has one hidden layer, while an MLP network can have one or several hidden layers. One of the most prominent characteristics of RBF networks is that the distance (such as the Euclidean distance) between the input pattern and the central vector is used as the input of the activation function, which is usually called the radial basis function. The role of the activation function is to introduce non-linearity into the network, which is the crucial aspect that makes the ANNs more powerful. One example of the radial basis function is the Gaussian function. Sigmoid functions and softmax functions are typically used as the nonlinear activation functions of the hidden nodes of an MLP network whose inputs are the inner product of an input pattern and a weight vector.

The operation frequency of the study in [19] is 2.427 GHz; the input of their ANNs are the 3D coordinates of the AP and receiving points, and the output is the predicted RSS. More complicated inputs are used in [20], where the

performances of RBF networks and MLP networks are also compared. The results show that the RBF networks obtain a slight improvement over the MLP networks of about 0.15 dB in the RMSE sense. Milijic et al. [21] present a hybrid-empirical neural (HEN) model for indoor and outdoor path loss prediction. Two MLP networks are used to estimate two important parameters in a log-distance form empirical model—the power loss coefficients and the floor penetration loss factor. In addition to the carrier frequency and TR-separations, the HEN model takes many other parameters affecting the EM propagation as the inputs of ANN, like the percentage of foliage areas in the propagation path, average height of foliage areas objects, and average height of buildings in the urban environment. In an attempt to prepare good features that are easy to learn, Yang and Lee [6] presented a neural network wave propagation loss model with the feature extraction algorithms, which can pre-process urban area digital elevation maps (DEM) to the inputs of ANN. The inputs of ANN include terrain penetration features, building penetration features, diffraction features, and reflected distances, which are calculated based on their algorithms. However, the input of their feature extraction algorithm still includes a lot of influencing factors of wave propagation, such as the antenna radiation pattern and varying distance elements. For the feature extraction, it is still difficult to acquire DEM data in a new urban area, and extensive computations of the feature extraction are likely inevitable. Moreover, although their work may provide some hints for indoor path loss modeling, their model is designed for outdoor urban areas.

In ANN-based path loss modeling, feature selection and extraction are the most critical parts that determine the accuracy in path loss prediction. The features used in ANN models usually contain many propagation environment configuration parameters, such as distance, the frequency of the carrier wave, terrain information, and so on. However, these features may not be the only ones that play important roles in obtaining an accurate model. They may also be extremely complicated to compute, even in a simple indoor scenario, thus leading to an intolerable amount of data pre-processing and feature extractions. This leads us to consider a deep learning model as an alternative method because it can be trained to learn to extract the features related to the propagation environment and to estimate the latent probability distribution of the measurement data.

### III. DEEP LEARNING-BASED PATH LOSS MODELING SYSTEM

#### A. Convolutional Neural Networks

CNNs are one of the most popular and powerful deep

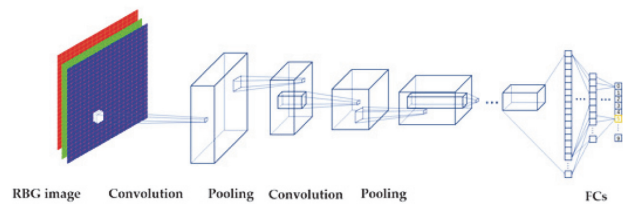


**Fig. 1.** The basic structure of a convolutional neural network.

neural network variants, and they typically involve more than two convolutional layers [22]. In CNNs, features are extracted automatically by the filters (or kernels) of convolutional layers, which can be used for classifications or regressions [23]. The filters can be regarded as the learnable weight matrix in convolutional layers. A CNN usually involves two additional crucial parts: pooling layers and fully connected (FC) layers, as shown in Fig. 1. The input of the CNN is RGB images. Then, convolution operations and pooling operations are performed in the following multiple convolutional layers. FC layers (FCs) are added to the final convolutional layers to execute classifications or regressions. Pooling layers can progressively reduce the size of the output of convolutional layers, which is called an activation map, as well as reduce the number of parameters to be calculated and learned during the training. Hence, a pooling layer can control overfitting. The pooling layer can also achieve spatial invariance of features by reducing the resolution of the activation maps. The activation maps are expected to contain the features extracted by the convolutional layer. Based on the features extracted by the upper convolutional layers, the FC layers can do the inference in the same manner as the traditional MLP networks with the supervision of the label(s).

A CNN can be trained to find the useful features of the objects in an input image by updating the weights associated with the filters, which has been demonstrated in our previous research of suburban path loss modeling [24, 25]. During the convolution process, a CNN filter moves from the top left of an input image to the bottom right of that image at a certain step size, which is called a stride. Fig. 2(a) illustrates the convolution process of CNNs. The size of the activation maps is usually smaller than the size of the convolutional layer. The neurons in the convolutional layers are typically arranged in three dimensions: width, height, and depth. The input of a typical CNN is three channels of RGB images. The number of output channels of a convolutional layer is the same as the number of filters. Here, we only show one channel as a simple example. Within each convolutional layer, input images are convolved with learnable filters. After the convolution process, the activation function will be applied to the output of the convolutional layer with an added bias. The most popular types of activation



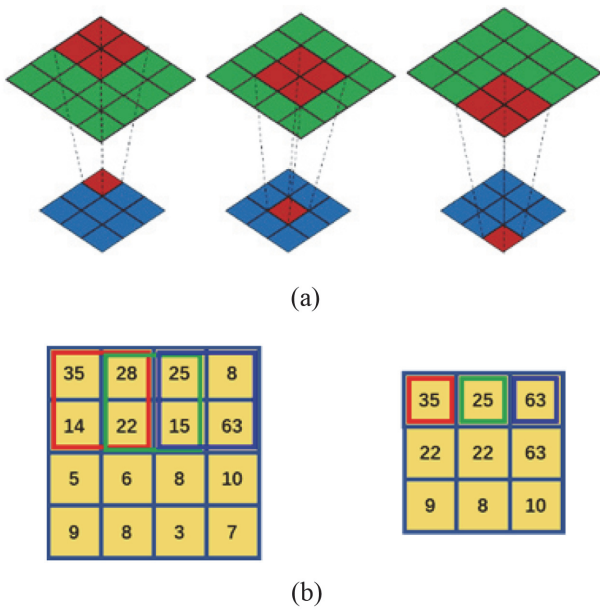


**Fig. 2.** Without a loss of generality and for simplicity, we show an example of the convolution and the pooling procedure with the single channel two-dimensional data. (a) The diagram of the convolutional process. (b) A max pooling example with a 2x2 filter and a stride size of one.

functions used in convolutional layers are the sigmoid (or logistic) function, Tanh (hyperbolic tangent), and the ReLU (rectified linear units) function. The activation function will also be used in the FC layer. In general, the  $j_{th}$  activation map in layer  $l$  can be defined as:

$$x_j^l = f(\sum_{i \in M_j} x_i^{l-1} w_{ij}^l + b_j^l) \tag{1}$$

where  $f(\cdot)$  is the activation function and  $M_j$  is the set of the input activation maps or input image channels, and each output activation map can be given an additive bias  $b_j^l$ . The inputs are convolved by different filters to multiple output activation maps by multiplying the neurons  $x_i^{l-1}$  of the  $j_{th}$  input activation maps in the  $(l-1)_{th}$  layer with the weight  $w_{ij}^l$  of the filter in  $l_{th}$ , and these connect the  $i_{th}$  output activation map and the  $j_{th}$  input activation map.

Given a volume of input neurons of shape  $W_1 \times H_1 \times D_1$ , four hyperparameters can be used to define the convolution operation: the number of filters  $K$ , the size of a filter  $F \times F$ , the stride size  $S$ , and the amount of zero-padding  $P$ . An output activation map of size  $W_2 \times H_2 \times D_2$  is produced after the convolution operation in the manner shown in the following equation.

$$\begin{cases} W_2 = \frac{W_1 - F + 2 \times P}{S} + 1 \\ H_2 = \frac{H_1 - F + 2 \times P}{S} + 1 \\ D_2 = K \end{cases} \tag{2}$$

The pooling is a down-sampling operation that can be performed on the activation maps by the pooling layer, which can combine multiple neurons in a square shape at one layer into a single neuron in the next layer. One of the most popular pooling methods is max pooling, which extracts the most prominent features of the activation maps, like edges, by taking only the maximum value from a fixed region of an activation map. Fig. 2(b) illustrates an example of a max pooling procedure of a 4x4 input (green) volume with a 2x2 (red) filter. The output (blue) volume will shrink into the small one shown at the bottom with the size of 3x3.

The calculation of pooling layers is almost the same as that for the convolutional layer, except that there is no padding. Given a volume of input activation maps with the shape as  $W_1 \times H_1 \times D_1$ , there are only three hyperparameters needed to define the pooling operation: the number of filters  $K$ , the size of the filters with the shape as  $F \times F$ , and the stride size  $S$ . After the pooling procedure in the pooling layer, a volume of size  $W_2 \times H_2 \times D_2$  is produced as follows:

$$\begin{cases} W_2 = \frac{W_1 - F}{S} + 1 \\ H_2 = \frac{H_1 - F}{S} + 1 \\ D_2 = K \end{cases} \tag{3}$$

After several convolutional layers and pooling layers, the neurons in the activation maps will be flattened into a neuron vector, which will serve as the input of the first FC layer. With a certain number of neurons in each FC layer, the final outputs can be inferred. The FC layers in CNNs work in the same way as the traditional MLP networks, except that the inputs of the first FC layer are the flattened high-level features from the last convolutional layer.

## B. Deep Learning-based Path Loss Modeling System Design

The architecture of the proposed deep learning-based path loss modeling system is illustrated in Fig. 3. The measurement data include the locations of the APs and the measurements as well as the corresponding RSS values. The main input of the proposed CNN path loss model is images generated by a novel input image generation algorithm known as the LAMS algorithm. The LAMS algorithm aims to extract the environmental features from the simplified floor plan. Since the TR-separation plays a significant role in path loss modeling, a distance neuron is appended to the first FC layer to make explicit the distance information to the CNN model. The CNN path loss model is trained to predict RSS based on the LAMS images and the TR-separation in the training phase. RMSE is used as the loss function

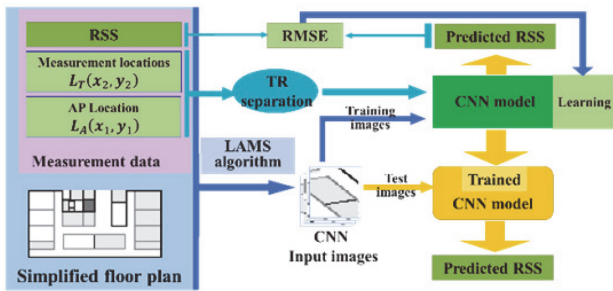


**Fig. 3.** Flow diagram of deep learning-based path loss modeling system.

of the CNN model. The trained CNN model can predict the RSS of a given location with the LAMS image and the TR-separation.

### C. Measurement and Data Collection

Fig. 4 shows the floor plan of the measurement environment, which hosts research laboratories, two seminar rooms with glass walls at the bottom center, and elevators, among other things [26]. The measurement area marked by the red rectangle with a size of 30 m × 15 m. One AP, which supports the IEEE 802.11.a/n 5.8 GHz Wi-Fi, was used as the transmitter in the measurement. A laptop was used as the Wi-Fi signal receiver. A measurement campaign was conducted during nights, when there was no movement of people or doors. Thus, the process is stationary [27, 28]. It is difficult to manually collect extensive measurements in a variational environment in practice. Still, at least 10 measurements were collected at each location 0.9 m apart from each

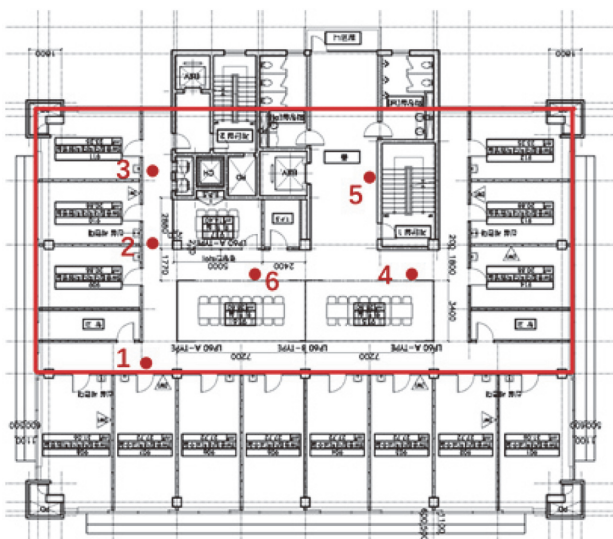


**Fig. 4.** The floor plan of the RSS measurement environment.

**Table 1.** The number of measurement data of APs

AP	The number of measurement data	Total number of measurement data
AP1	3,275	19,053
AP2	2,852	
AP3	2,795	
AP4	2,807	
AP5	3,682	
AP6	3,642	

other in order to average out the time fading effect. There are 236 measurement locations in the measurement area. Table 1 shows the numbers of measurement data of the APs. The RSS values were recorded by WirelessMon [29], which allows users to gather information about nearby wireless APs and hotspots in real time. APs are placed at six selected locations in the experiment, and these are marked as red dots in Fig. 4. The measured datasets are divided into two scenarios. The dataset of AP6 is used as the test dataset in Scenario 1. AP6 was placed at the center of the building, and the remaining APs were placed near the corners of the building. The dataset of AP1 is used as the test dataset in Scenario 2. AP1 was placed in the corner of the building, and it covers a larger LoS area than the other APs. The training dataset of these two scenarios covers different regions and different amounts sites with various propagation types. For example, the training dataset in Scenario 2 covers a smaller measurement area and contains more long-distance LoS measurement data than that of Scenario 1. The dataset of AP1 can be considered as a scenario with long LoS propagation paths, and it also covers a lot of NLoS sites, except for the sites located in the bottom long corridor, as shown in Fig. 4, while that of AP6 is a more general case wherein AP6 is located at the center. Therefore, Scenario 1 is a general indoor scenario and Scenario 2 is a specific scenario with long LoS sites and a lot of NLoS sites.

### D. CNN Input Images Generation: LAMS Algorithm

The inputs of CNNs should include sufficient environmental information of the path loss for the automatic feature extraction of convolutional layers so that the potential deep learning-based path loss model can learn the relationship between the inputs and outputs. The LAMS algorithm is designed to generate input images that include path loss environment information for CNN-based path loss modeling. The LAMS algorithm is analogous to a medical computed tomography scan, which uses many X-rays collected from different angles to generate repre-

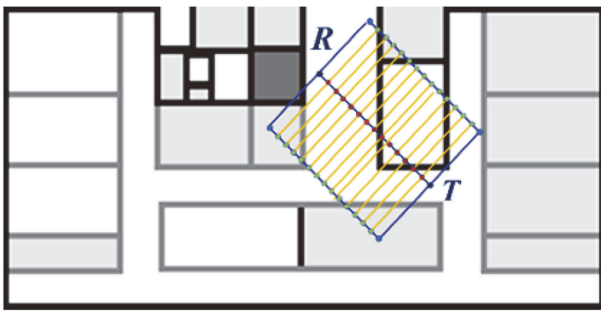


Fig. 5. LAMS algorithm.

representative images of a scanned object. As illustrated in Fig. 5 and Algorithm 1, a local area is defined as a rectangular shape region wherein the AP is located at the center of an edge and a measurement location is located at the center of the opposite side. Grey shading is used to indicate whether rooms are occupied. Grey and black lines represent foam and concrete walls, respectively.

As depicted in Fig. 5, the LAMS algorithm can abstract the environmental information of the path loss within the local area, which is defined as a region related to a pair consisting of an AP and a measurement location. The blue square and the yellow lines indicate the local area and the scan lines, respectively. The LAMS algorithm collects the pixels of the floor plan along multiple scan lines, which can be determined by the position of the local area. The AP (T) and a measurement receiver (R) are located at the edge centers and the opposite side of the local area, respectively. Specifically, the pixel values of the scan lines on a floor plan are copied as vectors. The size of a generated input image is pre-defined as  $(w, n)$ . Given the floor plan  $I_F$  and the locations of T and R, the LAMS algorithm proceeds as follows. First, the linear equation of line  $l_{TR}$  is calculated. Then, the locations of  $n$  points on  $l_{TR}$  are calculated. These  $n$  points, which are marked in red in Fig. 5, are regarded as the midpoints of  $n$  scan lines. The endpoint locations of each scan line perpendicular to  $l_{TR}$  are then calculated. Next, the  $w$  pixel values of the  $i^{th}$  scan line are saved as  $s_i$ . Finally, an input image can be generated by concatenating the pixel values set of scan lines  $s_i, i = 1, 2, 3, \dots, n$  together. Fig. 6 shows three generated input images that capture the building structures of the local area.

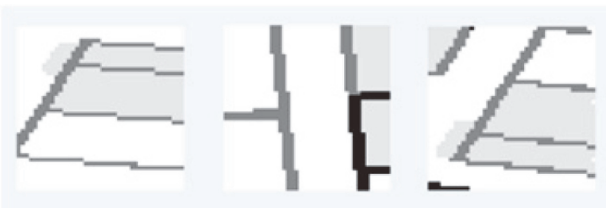


Fig. 6. Examples of generated input images.

Algorithm 1. LAMS algorithm

**Inputs:**

- Location of AP point  $T$
- Location of measurement  $R$
- Size of generated input image  $(w, n)$
- Image matrix of simplified floor plan  $I_F$

- 1: **Calculate the linear equation of**  $l_{TR}$
- 2: **Add**  $n$  **points on**  $l_{TR}$  **and determine the coordinates of these points**
- 3: **for**  $i = 1 : n$
- 4:     Calculate the endpoint coordinates of each scan line
- 5:     Copy  $w$  pixel values of the scan line on  $I_F$  and save them as  $s_i$
- 6: **end for**
- 7: **Integrate**  $s_i, i = 1, 2, 3, \dots, n$  **as a matrix**  $I_{LAMS}$
- 8: **Save the matrix**  $I_{LAMS}$  **as an input image**

**E. Design of CNN Model**

A CNN can learn the underlying functions of the Wi-Fi signal propagation by the automatic feature extraction of the convolutional layers. The distance neuron is appended to the flattened feature map that represents the path loss relevant features in the first FC layer to predict RSS. In this case, the size of the CNN input images is  $40 \times 40$ , which is designed to maintain the spatial information of the path loss environment and the directivity from the APs to the measurement locations.

There is no pooling layer between two adjacent convolutional layers. In general, the usage of pooling can decrease the parameters of the network, and it can thus accelerate the speed of training and avoid the overfitting problem. For example, in computer vision problems, the pooling operation helps CNN achieve spatial invariance. However, the introduction of pooling layers can lead to a loss of essential information in the input. In our case, we are attempting to maintain the spatial information of the measurement environment as well as the directivity from the AP to the measurement points. The size of the CNN input images in our experiment is  $40 \times 40$ , and they are simple small grey images. If there is no pooling layer after the convolutional layers, the size of activation maps can be kept unchanged, and useful features can thus be expected to be extracted from the CNN input images, which can be good for the reasoning and calculation on the FC layers. Consequently, pooling layers are not used in our CNN models.

The prediction performance of a CNN model is

**Table 2.** Four types of convolutional layers

Layer type	Parameters of convolutional layers			
	Input channel	Output channel	Kernel size	Stride size
$C_1$	3	6	4	3
$C_2$	6	3	3	2
$C_{m_j}$	3	3	2	1
$C_f$	3	2	2	2

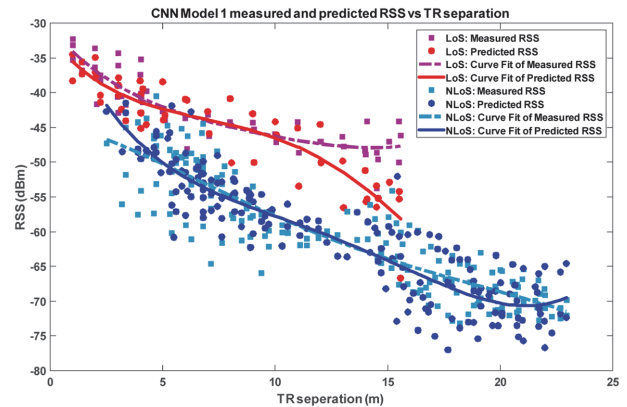
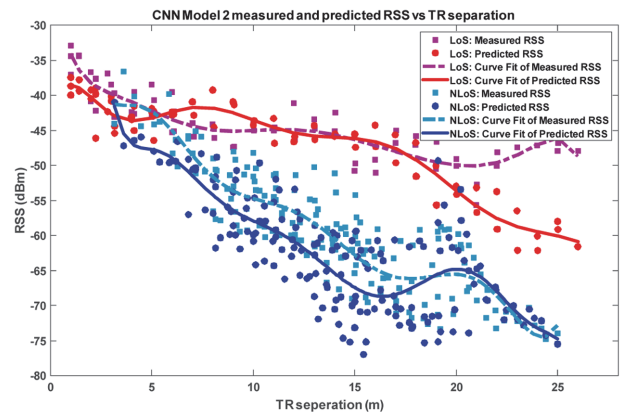
primarily dependent on its structure, such as the number of convolutional layers and FC layers, and the number and size of filters [30]. Table 2 details the four types of convolutional layers, which are denoted as  $C_1$ ,  $C_2$ ,  $C_{m_j}$ , and  $C_f$ .  $C_1$ ,  $C_2$ , and  $C_f$  are the first, second, and final convolutional layers, respectively.  $C_{m_j}$  is the  $j$ th  $C_m$  convolutional layer, where  $C_m$  indicates that it is between the  $C_2$  and  $C_f$  layers, and it is a middle convolutional layer. Using the ‘‘SAME’’ padding method, the activation maps of the input and output of  $C_{m_j}$  ( $j > 1$ ) layers are of the same size. Thus, the size of the activation maps can be maintained, which is conducive to the implementation of deeper CNN structures.

Zero-padding is also introduced. The padding method is set as ‘‘VALID’’ in the first two and the last convolutional layers, while ‘‘SAME’’ padding is used in the rest of the convolutional layers. ‘‘VALID’’ means there is no padding, which can make the size of the activation map shrink fast. ‘‘SAME’’ padding can make the spatial size of the output volumes the same as the input volumes. ‘‘SAME’’ padding tries to pad evenly left and right, but if the number of columns to be added is odd, it will add an extra column to the right. The activation functions used in the convolutional layers and FCs are the ReLU function [31]. The range of the measurement RSS values is between -100 dBm and -10 dBm. Due to the unilateral suppression attribute of ReLU, the negative measurement RSS values cannot be directly used as labels. Therefore, the label data should be shifted into positive values. For example, if the RSS value is -30 dBm, the label value will be 70 if we add 100 to it. The loss function used in the experiment is the RMSE. Another design decision is the choice of the training algorithm. Here, the Adam algorithm is chosen (learning rate  $lr = 0.001$ ,  $\beta_1 = 0.9$ ,  $\beta_2 = 0.99$ ,  $\epsilon = e^{-8}$ ) [32]. TensorFlow is used to implement our CNN model [33]. Since the training datasets of the two scenarios contain different environmental information and propagation types, we designed two CNN models with various network structures for two scenarios. The performances of the different CNN structures in the test are illustrated in [26]. CNN Model 1, which is designed for Scenario 1, has five convolutional layers (including two  $C_m$  layers), and seven and three neurons in the first and second

hidden FC layers, respectively. CNN Model 2, which is designed for Scenario 2, has 10 convolutional layers (including seven  $C_m$  layers), and 15 and five neurons in the hidden FC layers, respectively.

## IV. EXPERIMENTAL RESULTS

CNN models with different structures were trained and tested in two scenarios to evaluate the performance of the proposed deep learning-based path loss model. Comparisons between the predicted RSSs of CNN models and the measured RSSs with respect to the TR-separation as well as those in Scenario 1 and Scenario 2 are shown in Figs. 7 and 8. We perform polynomial curve-fitting on both the measured RSS values and the predicted RSS values for improved visualization. Given a fixed location of an AP and a measurement location, if the center line  $l_{TR}$  of CNN input images generated by the LAMS algorithm has pixel values that are not white colour, then this measurement point will be thought of as an NLoS point; otherwise, it is thought of as an LoS point. The polynomial fit degrees of CNN Model 1 and CNN Model 2 were set to 4 and 9,


**Fig. 7.** Performance evaluation of CNN Model 1.

**Fig. 8.** Performance evaluation of CNN Model 2.

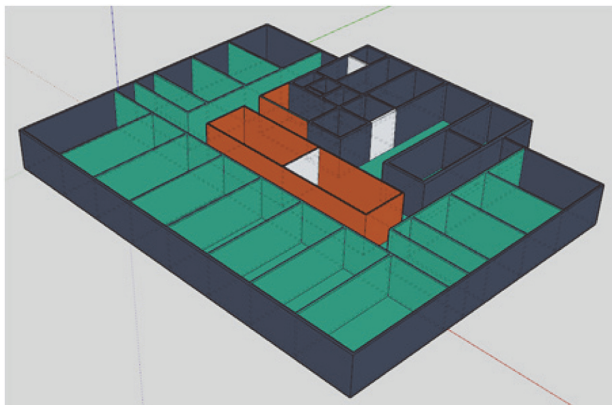




**Fig. 9.** The SketchUp 3D map of the measurement environment.

respectively. The difference between the predicted and measured RSS values of CNN Model 1 is smaller than that of CNN Model 2. For both scenarios, the predicted RSS of CNN models can separate the LoS and NLoS scenarios, which indicates that the proposed CNN-based path loss model has a good interpretation of the LoS and NLoS propagation.

The test RMSEs of CNN Model 1 and CNN Model 2 are 3.94 dB and 5.32 dB, respectively. The prediction errors of CNN models are larger when an LoS Rx is far from the Tx and close to the corner, as shown in Figs. 7 and 8. According to [34], because of the reflection of radio waves caused by walls behind Rx and perpendicular to the T-R direction, the RSS values at LoS sites in the corner are larger than the others. CNN Model 2 could not perform as good as CNN Model 1 since the LAMS images do not contain information on the environment behind. Table 3 summarizes the percentiles of absolute RSS prediction errors at 2, 5, and 10 dB in CNN Model 1 and Model 2 with a total of 236 measurement points. The results show that the absolute errors smaller than 5 and 10 dB of CNN Model 1 are about 7% higher than those of CNN Model 2. This suggests that the CNN models can achieve a good generalization capability when they are trained with a set of training samples covering a sufficient range of different radio propagation environments.

With incomplete information of the propagation environment, CNN Model 2 achieves the best performance when

**Table 3.** The absolute error of predicted RSS of CNN Model 1, CNN Model 2, and the 3D ray-tracing method

Absolute error (dB)	Percentile %		
	CNN Model 1	CNN Model 2	Ray-tracing
<2	38.33	37.01	31.36
<5	77.97	70.11	67.82
<10	98.05	91.76	88.30

it has 10 convolutional layers as well as 15 and five neurons in hidden FC layers. The CNN-based path loss model requires additional parameters to model the underlying function of the path loss when there is limited environment information.

Moreover, we validated the performance of the CNN-based path loss model by comparing it with the 3D ray-tracing method using a ray-tracing simulator developed by Beijing Jiao Tong University [12]; it can trace the direct, reflected, scattered, and diffracted rays, and it is validated and calibrated by a large number of measurements from sub-6 GHz to terahertz (THz) band. The ray-tracing method is a popular approach for channel modeling because it can simulate the propagation mechanisms of wireless channels [35, 36]. Fig. 9 shows a 3D map of the measurement environment that is built by SketchUp [37]. The black walls on the edge of the building are concrete walls and the green walls are foam walls. Note that the floor is also green, which indicates that we assume that the materials of the floor are the same material as the foam wall, and the path loss between floors is not considered. The white and orange walls are made from metal and glass materials. The hyperparameters used in the 3D ray-tracing simulation are listed in Tables 4 and 5, including the parameters of the transmitter (AP) and

**Table 4.** Configurations of transmitter and receiver

	Value
Transmitter	
Height	1.7 m
Transmission power	17 dBm
Channel	40
Center frequency	5.8 GHz
Antenna pattern	Vertical omnidirectional polarization
Receiver	
Height	0.92 m
Number of discrete measurement locations	236
Antenna pattern	Vertical omnidirectional polarization

**Table 5.** EM properties of building materials

Materials	Directive		Real permittivity	Imaginary permittivity
	S	Sigma		
Wall				
Foam	0.0026	18	1.1955	0.4894
Concrete	0.0018	50	1.9155	0.0568
Metal	0.0020	30	1	10000000
Glass	1.0538	24	0.0025	5.5106

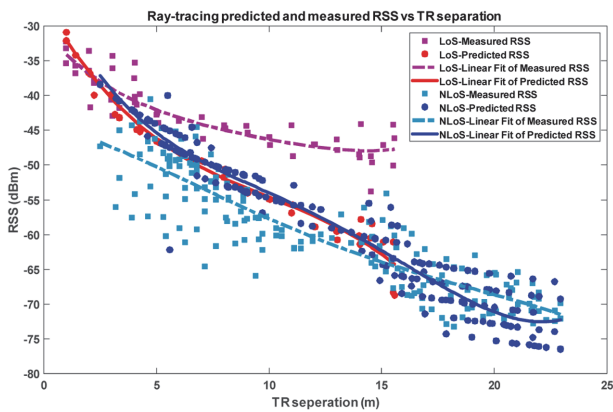


Fig. 10. Performance evaluation of 3D ray-tracing method.

receivers (laptops in different measurement points) and the EM properties of the building structure materials that determine the energy contribution of each ray when rays interact with the material surfaces. The transmission power of the transmitter used to compute the path loss values both for the CNN models and the 3D ray-tracing model was -17 dBm. The directive attributes include two parameters, the S factor and Sigma, which are used to calculate the attenuation of reflection and the pattern size of scattering by the Directive Model [12, 38], respectively. The value of real permittivity is also used as the S factor when calculating the scattering with the Lambertian Model.

The simulation result of the 3D ray-tracing method is shown in Fig. 10. The test dataset of Scenario 1 was used to evaluate the 3D ray-tracing method because Scenario 1 is more representative than Scenario 2 due to the former's wider variety of propagation environment. The RMSE between the measured RSS and the predicted RSS values generated by the 3D ray-tracing method is 5.85 dB. One can see that given the limited nature of the environmental information (just the floor plan), the predicted RSS values of the 3D ray-tracing method are less accurate than those of the CNN models, and 3D ray-tracing methods fail to make equally accurate predictions for a relatively simple indoor environment. The distribution of predicted RSS values is very narrow. The fitting curve of RSS prediction made by the 3D ray-tracing method cannot separate LoS and NLoS scenarios, which implies that the robustness of the ray-tracing method is not as good as our proposed CNN method when the floor plan is the only available propagation environment information.

The percentiles of absolute RSS prediction errors at 2, 5, and 10 dB of the 3D ray-tracing method are summarized in Table 5. The percentiles of the absolute RSS predicted error of the 3D ray-tracing method are at least 8 dB smaller than those predicted by the proposed CNN models. From the above comparison and illustration, it can be seen that the proposed CNN-based path loss prediction model outperforms the 3D ray-tracing method in terms of robustness, generalization, and accuracy.

## V. CONCLUSION

We developed a novel deep learning-based indoor path loss modeling approach for 5.8 GHz Wi-Fi. Based on a floor plan and measurement data, the LAMS input image generation algorithm for CNNs was proposed. Two CNN-based path loss models with different network structures were presented. The experimental results demonstrated the superior performance of the proposed path loss models over the 3D ray-tracing method. In our future research, we plan to study deep learning-based path loss models for the new-generation Wi-Fi operating in the 60 GHz frequency band as well as 5G systems in both indoor scenarios and outdoor scenarios involving environmental changes. We will also generate new training images containing more information on the propagation environment for training.

## ACKNOWLEDGMENTS

This research was supported by the MIST, Korea, under the National Program for Excellence in SW supervised by the IITP (No. 2017-0-00096).

## REFERENCES

1. A. Bhuvaneshwari, R. Hemalatha, and T. Satyasavithri, "Path loss prediction analysis by ray tracing approach for NLOS indoor propagation," in *Proceedings of 2015 International Conference on Signal Processing and Communication Engineering Systems*, Guntur, India, 2015, pp. 486-491.
2. H. K. Rath, S. Timmadasari, B. Panigrahi, and A. Simha, "Realistic indoor path loss modeling for regular WiFi operations in India," in *Proceedings of 2017 23rd National Conference on Communications (NCC)*, Chennai, India, 2017, pp. 1-6.
3. I. Vilovic and N. Burum, "Neural network prediction of signal strength for irregular indoor environments," *Automatika*, vol. 56, no. 1, pp. 55-68, 2015. <https://doi.org/10.7305/automatika.2015.04.463>
4. B. O. H. Akinwale and J. J. Biebuna, "Comparative analysis of empirical path loss model for cellular transmission in rivers state," *American Journal of Engineering Research*, vol. 2, no. 8, pp. 24-31, 2013.
5. S. I. Popoola, E. Adetiba, A. A. Atayero, N. Faruk, and C. T. Calafate, "Optimal model for path loss predictions using feed-forward neural networks," *Cogent Engineering*, vol. 5, no. 1, article no. 1444345, 2018. <https://doi.org/10.1080/23311916.2018.1444345>
6. S. Yang and H. Lee, "Feature extraction for neural network wave propagation loss models from field measurements and digital elevation map," *IEICE Transactions on Electronics*, vol. 82, no. 7, pp. 1260-1266, 1999.
7. I. Goodfellow, Y. Bengio, A. Courville, and Y. Bengio, *Deep Learning*. Cambridge, MA: MIT Press, 2016.

8. S. S. Sidhu, A. Khosla, and A. Sharma, "Implementation of 3-D ray tracing propagation model for indoor wireless communication," *International Journal of Electronics Engineering*, vol. 4, no. 1, pp. 43-47, 2012.
9. Q. Wang, B. Ai, K. Guan, D. W. Matolak, R. He, and X. Zhou, "Ray-based statistical propagation modeling for indoor corridor scenarios at 15 GHz," *International Journal of Antennas and Propagation*, vol. 2016, article no. 2523913, 2016. <https://doi.org/10.1155/2016/2523913>
10. K. Guan, Z. Zhong, B. Ai, and T. Kurner, "Deterministic propagation modeling for the realistic high-speed railway environment," in *Proceedings of 2013 IEEE 77th Vehicular Technology Conference (VTC Spring)*, Dresden, Germany, 2013, pp. 1-5.
11. Laboratory of Antenna Propagation and Channel, "CloudRT: High Performance Antenna, Propagation and Channel Modeling Platform," 2021; <http://cn.raytracer.cloud:9090/>.
12. D. He, B. Ai, K. Guan, L. Wang, Z. Zhong, and T. Kurner, "The design and applications of high-performance ray-tracing simulation platform for 5G and beyond wireless communications: a tutorial," *IEEE Communications Surveys & Tutorials*, vol. 21, no. 1, pp. 10-27, 2018.
13. R. Akl, D. Tummala, and X. Li, "Indoor propagation modeling at 2.4 GHz for IEEE 802.11 networks," in *Proceedings of the 6th IASTED International Multi-conference on Wireless and Optical Communications*, Banff, Canada, 2006.
14. X. Zhao, S. Geng, and B. M. Coulibaly, "Path-loss model including LOS-NLOS transition regions for indoor corridors at 5 GHz [wireless corner]," *IEEE Antennas and Propagation Magazine*, vol. 55, no. 3, pp. 217-223, 2013.
15. Y. Wang, W. J. Lu, and H. B. Zhu, "An empirical path-loss model for wireless channels in indoor short-range office environment," *International Journal of Antennas and Propagation*, vol. 2012, article no. 636349, 2016. <https://doi.org/10.1155/2012/636349>
16. A. El-Keyi, H. U. Sokun, T. N. Nguyen, Q. Ye, H. J. Zhu, and H. Yanikomeroglu, "A novel probabilistic path loss model for simulating coexistence between 802.11 and 802.15.4 networks in smart home environments," in *Proceedings of 2017 IEEE 28th Annual International Symposium on Personal, Indoor, and Mobile Radio Communications (PIMRC)*, Montreal, Canada, 2017, pp. 1-5.
17. H. S. Jo, C. Park, E. Lee, H. K. Choi, and J. Park, "Path loss prediction based on machine learning techniques: principal component analysis, artificial neural network and Gaussian process," *Sensors*, vol. 20, no. 7, article no. 1927, 2020. <https://doi.org/10.3390/s20071927>
18. S. I. Popoola, A. Jefia, A. A. Atayero, O. Kingsley, N. Faruk, O. F. Oseni, and R. O. Abolade, "Determination of neural network parameters for path loss prediction in very high frequency wireless channel," *IEEE Access*, vol. 7, pp. 150462-150483, 2019.
19. I. Vilovic and N. Burum, "A comparison of MLP and RBF neural networks architectures for electromagnetic field prediction in indoor environments," in *Proceedings of the 5th European Conference on Antennas and Propagation (EUCAP)*, Rome, Italy, 2011, pp. 1719-1723.
20. I. Popescu, D. Nikitopoulos, P. Constantinou, and I. Nafornita, "Comparison of ANN based models for path loss prediction in indoor environment," in *Proceedings of the 64th IEEE Vehicular Technology Conference (VTC Fall)*, Montreal, Canada, 2006, pp. 1-5.
21. M. Milijic, Z. Stankovic, and I. Milovanovic, "Hybrid-empirical neural model for indoor/outdoor path loss calculation," in *Proceedings of 2011 10th International Conference on Telecommunication in Modern Satellite Cable and Broadcasting Services (TELSIKS)*, Nis, Serbia, 2011, pp. 548-551.
22. J. Wu, "Introduction to convolutional neural networks," 2017; <https://cs.nju.edu.cn/wujx/paper/CNN.pdf>.
23. Z. Q. Zhao, P. Zheng, S. T. Xu, and X. Wu, "Object detection with deep learning: a review," *IEEE Transactions on Neural Networks and Learning Systems*, vol. 30, no. 11, pp. 3212-3232, 2019.
24. H. Cheng, S. Ma, and H. Lee, "CNN-based mmWave path loss modeling for fixed wireless access in suburban scenarios," *IEEE Antennas and Wireless Propagation Letters*, vol. 19, no. 10, pp. 1694-1698, 2020.
25. H. Cheng, S. Ma, H. Lee, and M. Cho, "Millimeter wave path loss modeling for 5G communications using deep learning with dilated convolution and attention," *IEEE Access*, vol. 9, pp. 62867-62879, 2021.
26. H. Cheng, H. Lee, and S. Ma, "CNN-based indoor path loss modeling with reconstruction of input images," in *Proceedings of 2018 International Conference on Information and Communication Technology Convergence (ICTC)*, Jeju, South Korea, 2018, pp. 605-610.
27. B. C. Liu, K. H. Lin, and J. C. Wu, "Analysis of hyperbolic and circular positioning algorithms using stationary signal-strength-difference measurements in wireless communications," *IEEE Transactions on Vehicular Technology*, vol. 55, no. 2, pp. 499-509, 2006.
28. K. Kaemarungsi and P. Krishnamurthy, "Properties of indoor received signal strength for WLAN location fingerprinting," in *Proceedings of the 1st Annual International Conference on Mobile and Ubiquitous Systems: Networking and Services*, Boston, MA, 2004, pp. 14-23.
29. SketchUp: 3D design software, <https://www.sketchup.com/>.
30. W. S. Ahmed, "The impact of filter size and number of filters on classification accuracy in CNN," in *Proceedings of 2020 International Conference on Computer Science and Software Engineering (CSASE)*, Duhok, Iraq, 2020, pp. 88-93.
31. V. Nair and G. E. Hinton, "Rectified linear units improve restricted Boltzmann machines," in *Proceedings of the 27th International Conference on Machine Learning (ICML)*, Haifa, Israel, 2010, pp. 807-814.
32. D. P. Kingma and J. Ba, "Adam: a method for stochastic optimization," 2014; <https://arxiv.org/abs/1412.6980>.
33. M. Abadi, A. Agarwal, P. Barham, E. Brevdo, Z. Chen, C. Citro, et al., "TensorFlow: large-scale machine learning on heterogeneous distributed systems," 2016; <https://arxiv.org/abs/1603.04467>.
34. W. Gu, M. A. Kashani, and M. Kavehrad, "Multipath reflections analysis on indoor visible light positioning system," 2015; <https://arxiv.org/abs/1504.01192>.
35. T. Abbas, J. Nuckelt, T. Kumer, T. Zemen, C. F. Mecklenbräuker, and F. Tufvesson, "Simulation and measurement-based vehicle-to-vehicle channel characterization: accuracy and constraint analysis," *IEEE Transactions on Antennas and*

- Propagation*, vol. 63, no. 7, pp. 3208-3218, 2015.
36. S. Hur, S. Baek, B. Kim, Y. Chang, A. F. Molisch, T. S. Rappaport, K. Haneda, and J. Park, "Proposal on millimeter-wave channel modeling for 5G cellular system," *IEEE Journal of Selected Topics in Signal Processing*, vol. 10, no. 3, pp. 454-469, 2016.
37. A. Chopra, *Introduction to Google SketchUp*. Hoboken, NJ: John Wiley & Sons, 2012.
38. V. Degli-Esposti, F. Fuschini, E. M. Vitucci, and G. Falciasecca, "Measurement and modelling of scattering from buildings," *IEEE Transactions on Antennas and Propagation*, vol. 55, no. 1, pp. 143-153, 2007.



**Shengjie Ma** <https://orcid.org/0000-0001-7506-8120>

---

Shengjie Ma was born in Linyi, Shandong, China, in 1994. She received the B.S. degree from the Department of Software Engineering, Qingdao University of Science and Technology, in 2016. She is currently pursuing the Ph.D. degree in computer engineering at Kwangwoon University, Seoul, South Korea. Her research interests include deep learning, vehicular positioning and path loss modeling.



**Hong Cheng** <https://orcid.org/0000-0002-2139-9108>

---

Hong Cheng was born in Qingdao, Shandong, China, in 1993. He received the B.S. degree from the Department of Internet of Things Engineering, Qingdao University of Science and Technology, in 2016. He is currently pursuing the Ph.D. degree in computer engineering at Kwangwoon University, Seoul, South Korea. His research interests include deep learning and path loss modeling.



**Hyukjoon Lee** <https://orcid.org/0000-0001-7624-2020>

---

Hyukjoon Lee was born in Seoul, South Korea, in 1963. He received the B.S. degree in computer science from the University of Michigan, Ann Arbor, USA, in 1987, and the M.S. and Ph.D. degrees in computer and information science from Syracuse University, in 1989 and 1993, respectively. Since 1994, he has been working as a Senior Researcher with Samsung Electronics. In 1996, he joined the Faculty of the Department of Computer Engineering, Kwangwoon University. His research interests include machine learning, mobile and wireless networks, ITS, and smart healthcare systems.